Journal of Receptors and Signal Transduction

ISSN: 1079-9893 (Print) 1532-4281 (Online) Journal homepage: http://www.tandfonline.com/loi/irst20

Natural polyphenolic inhibitors against the antiapoptotic BCL-2

Sharad Verma, Aditi Singh, Anchala Kumari, Chetna Tyagi, Sukriti Goyal, Salma Jamal & Abhinav Grover

To cite this article: Sharad Verma, Aditi Singh, Anchala Kumari, Chetna Tyagi, Sukriti Goyal, Salma Jamal & Abhinav Grover (2017): Natural polyphenolic inhibitors against the antiapoptotic BCL-2, Journal of Receptors and Signal Transduction, DOI: 10.1080/10799893.2017.1298129

To link to this article: http://dx.doi.org/10.1080/10799893.2017.1298129

Published online: 06 Mar 2017.

JOURNAL OF RECEPTORS AND SIGNAL TRANSDUCTION, 2017
http://dx.doi.org/10.1080/10799893.2017.1298129

Taylor & Francis
Taylor & Francis Group

RESEARCH ARTICLE

Natural polyphenolic inhibitors against the antiapoptotic BCL-2

Sharad Verma[a], Aditi Singh[b], Anchala Kumari[b], Chetna Tyagi[a], Sukriti Goyal[c], Salma Jamal[c] and Abhinav Grover[a]

[a]School of Biotechnology, Jawaharlal Nehru University, New Delhi, India; [b]Department of Biotechnology, TERI University, Vasant Kunj, New Delhi, India; [c]Department of Bioscience and Biotechnology, Banasthali University, Tonk, Rajasthan, India

ABSTRACT

The apoptotic mechanism is regulated by the BCL-2 family of proteins, such as BCL-2 or Bcl-xL, which block apoptosis while Bad, Bak, Bax, Bid, Bim or Hrk induce apoptosis. The overexpression of BCL-2 was found to be related to the progression of cancer and also providing resistance towards chemotherapeutic treatments. In the present study, we found that all polyphenols (apigenin, fisetin, galangin and luteolin) bind to the hydrophobic groove of BCL-2 and the interaction is stable throughout MD simulation run. Luteolin was found to bind with highest negative binding energy and thus, claimed highest potency towards BCL-2 inhibition followed by fisetin. The hydrophobic interactions were found to be critical for stable complex formation as revealed by the vdW energy and ligplot analysis. Finally, on the basis of data obtained during the study, it can be concluded that these polyphenols have the potential to be used as lead molecules for BCL-2 inhibition.

ARTICLE HISTORY
Received 2 June 2016
Accepted 15 February 2017

KEYWORDS
BCL-2; polyphenols; molecular docking; molecular dynamics simulation; free energy calculation; principal component analysis

Introduction

Apoptosis or programed cell death is a molecular event by which cell termination occurs after performing its physiological roles. The apoptotic mechanism is regulated by the BCL-2 family of proteins (1,2). BCL-2, Bcl-xL, Bcl-w or Mcl-1 are known to block apoptosis, while Bad, Bak, Bax, Bid, Bim or Hrk perform the induction of apoptosis. The elevated expression of BCL-2 and Bcl-xL proteins was found to be related to the progression of cancer and also provides resistance towards chemotherapeutic treatments (3). BCL-2 family proteins are characterized by BCL-2 homology (BH) domains (four conserved sequences of amino acids) (4–8). BCL-2 family proteins are grouped into three distinct subclasses: (1) the BH3-only proteins (only BH3 is present) such as Bim, Bad, Puma, and Noxa that communicate pro-death signals to Bax, and Bak and activate them (9,10), (2) proteins constituting BH1 to BH3 domains, such as Bax and Bak, that induce apoptosis by the outer mitochondrial membrane destabilization and facilitating release of cytochrome c from mitochondria to the cytosol (11,12), (3) proteins constituting all the four BH1 to BH4 domains, such as BCL-2, Bcl-xL, Bcl-w, Mcl-1, A1 and Bcl-B, that suppress the activation of Bax/Bak (13–17). BCL-2 forms a hetero-dimer with Bax. The BH3 region of Bax and the BH1–BH3 regions of BCL-2 are required for complex formation (18–22). The BCL-2 protein formed a hydrophobic groove by the BH1–BH3 regions which interacts with hydrophobic residues of an amphipathic α-helix formed by Bax BH3 region (23,24). The antiapoptotic proteins (BCL-2, Bcl-xL and Mcl-1) are primarily constituted of two central hydrophobic helices surrounded by amphipathic helices (25,26). Helices α2, α3, α4 and α5 form a hydrophobic groove (27).

We selected four plant-derived polyphenols (natural phytochemicals) for possible inhibition of BCL-2. Apigenin is widely found in many fruits and vegetables including chamomile, parsley, onions, tea, orange and wheat sprouts (28). Fisetin is present in strawberries, apples, persimmons, kiwis, cucumbers and onions (29). Galangin is a found in *Alpinia officinarum* (lesser galangal) (30). Luteolin is found in high concentration in peanut hulls and in *Reseda luteola L.* (the Dyer's weld) (31,32). Structures of polyphenols are shown in Figure 1. Our previous study reported BCL-2–Bax complex disruption effect by quercetin and taxifolin (33). Molecular dynamics simulation studies have significant contribution in enhancing knowledge of molecular mechanisms and the mode of binding of inhibitors (33–38). These computational drug discovery approaches have been very popular now and implemented on a major scale to minimize the search space (39–42). The molecular docking, molecular dynamics simulation and MM/PBSA-binding energy were performed to elucidate the potential of polyphenols in inhibition of the BCL-2.

Computational methods

Molecular docking was performed by using Molecular docking suite AutoDock 4.0. The crystal structure of BCL-2 (PDB ID: 1YSW) (43) was obtained from the RCSB protein data bank. The structures of polyphenols (apigenin, fisetin, galangin and luteolin) were generated from SMILES strings. All the heteroatoms were removed during the preparation of protein coordinate file. All the missing atoms were repaired by AutoDock. Adaptive local search based Lamarkian genetic algorithm was used as a search parameter. Short range van

CONTACT Abhinav Grover abhinavgr@gmail.com, agrover@jnu.ac.in School of Biotechnology, Jawaharlal Nehru University, New Delhi, 110067, India

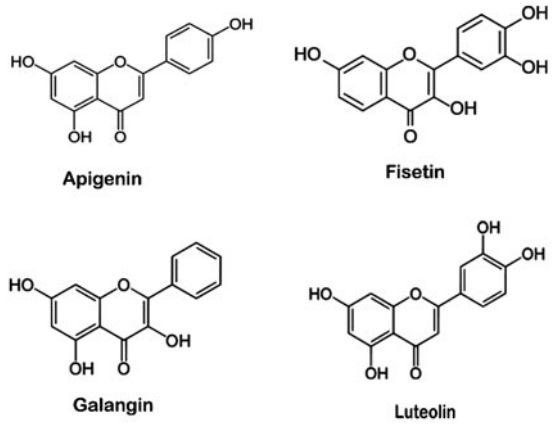

Figure 1. Structure of polyphenols.

der Waals and electrostatic interactions, hydrogen bonding, entropy losses were included for energy-based AutoDock scoring function (44,45). In the study, Lamarckian GA parameters that were used are number of runs, 20; population size, 150; the maximum number of eval, 250,00,000; the number of generations, 27,000; rate of gene mutation, 0.02; and the rate of cross over, 0.8. Blind docking was carried out using a cubic grid size of 126^3 along the X, Y and Z axes with 0.375 Å spacing. RMS cluster tolerance was set to 2.0 Å.

Molecular dynamics simulation

MD simulation of the complex was carried out using the GROMOS96 43a1 force field (46,47) of the GROMACS 4.5.5 package. Autodock generated lowest binding energy (most negative) docking conformation of BCL-2-polyphenol complex which was taken as initial conformation for MD simulation. The topology parameters of proteins were created by means of the Gromacs program. The topology parameters of taxifolin were built using the Dundee PRODRG server (48). The complex was immersed in a cubic box of extended simple point charge water molecules (49,50). Energy minimization was performed using the steepest descent method of 10,000 steps followed by the conjugate gradient method for 10,000 steps to release conflicting contacts. Position-restrained dynamics simulation (equilibration phase) (NVT and NPT) of the system was done at 300 K for 200 ps followed by MD production run for 15 ns. For the purpose of analysis, the atom coordinates were recorded every 1.0 ps during the MD simulation. All the structural images were generated using Chimera (51).

Binding free energy calculations

Binding free energies calculations was performed from the snapshots of MD trajectory using the molecular mechanics Poisson Boltzmann surface area (MM/PBSA) method (52). The binding free energies of the polyphenols-BCL-2 complexes were analyzed by taking snapshot at an interval of 1.5 ps from 13 to 15 ns MD simulations during equilibrium phase, using g_mmpbsa tool of Gromacs (53).

Particularly, the binding free energy of ligand-protein complex in solvent was expressed as follows:

$$\Delta G_{\text{binding}} = G_{\text{complex}} - (G_{\text{protein}} + G_{\text{ligand}})$$

where G_{complex} is the total free energy of the protein-ligand complex, G_{protein} and G_{ligand} are total energy of separated protein and ligand in solvent, respectively. The free energy for each individual G_{complex}, G_{protein} and G_{ligand} were estimated by:

$$G_x = E_{\text{MM}} + G_{\text{solvation}}$$

where x is the protein, ligand or complex. E_{MM} is the average molecular mechanics potential energy in vacuum and $G_{\text{solvation}}$ is free energy of solvation. The molecular mechanics potential energy was calculated in vacuum as following:

$$E_{\text{MM}} = E_{\text{bonded}} + E_{\text{nonbonded}} = E_{\text{bonded}} + (E_{\text{vdw}} + E_{\text{elec}})$$

where E_{bonded} is bonded interaction including of bond, angle, dihedral and improper interactions and $E_{\text{nonbonded}}$ is non-bonded interactions consisting of van der Waals (E_{vdw}) and electrostatic (E_{elec}) interactions. ΔE_{bonded} is always taken as zero (54).

The solvation free energy ($G_{\text{solvation}}$) was estimated as the sum of electrostatic solvation free energy (G_{polar}) and apolar solvation free energy (G_{nonpolar}):

$$G_{\text{solvation}} = G_{\text{polar}} + G_{\text{nonpolar}}$$

where G_{polar} was computed using the Poisson–Boltzmann (PB) Equation (52) and G_{nonpolar} was estimated from the solvent-accessible surface area (SASA) as followed:

$$G_{\text{nonpolar}} = \gamma\ \text{SASA} + \text{b}$$

where γ is a coefficient related to surface tension of the solvent and b is fitting parameter.

Principal component analysis (PCA)

The dominant and collective modes of the protein atom displacement from the overall dynamics of the MD trajectory were obtained by principal component analysis (PCA). The Gromacs in-built tool g_covar and g_anaeig were used to yield the eigen values and the eigen vectors, respectively (55). Porcupine plots were generated by PYMOL (56).

Results and discussion

Molecular docking results revealed that apigenin, fisetin, galangin and luteolin bind to the hydrophobic groove of BCL-2 with lowest binding energy (most negative) with values −5.67, −6.02, −5.18 and −6.59 kcal/mol, respectively. These docking conformation of BCL-2-polyhenol complexes, generated by Autodock, were taken as initial conformation for MD simulation. Figure 2(A) shows that the RMSD profiles were always less than 0.70 nm and stable for all ligands bound to BCL-2 backbone during the entire simulation suggesting the suitability of MD simulation run. Figure 2(B) shows the RMSD profile of polyphenols. The minimum distance calculated between BCL-2 and polyphenols is shown in Figure 3(A). Luteolin was found to be the closest with some fluctuations. Rest all polyphenols showed nearly steady distance. All BCL-2

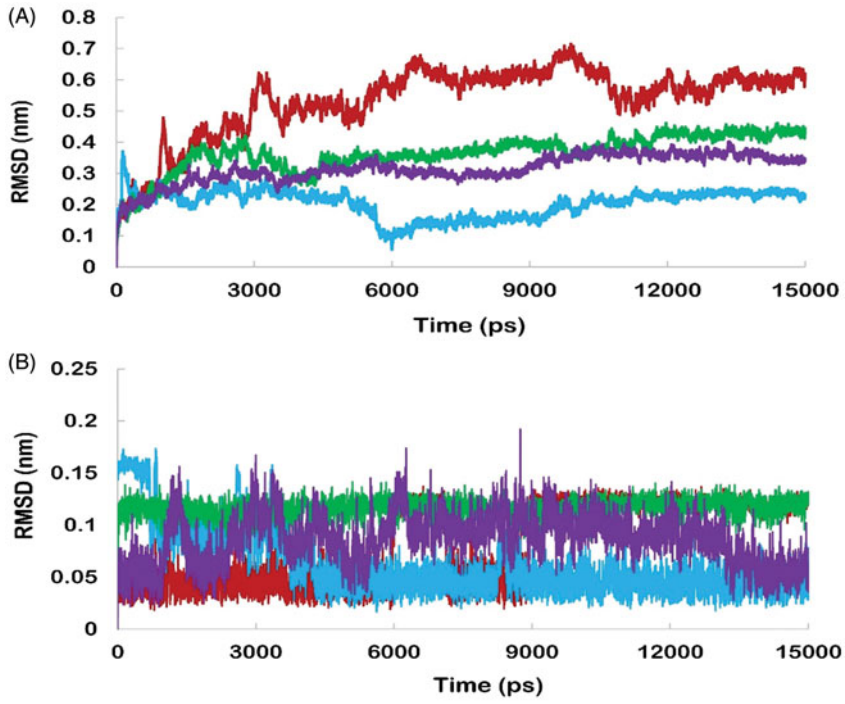

Figure 2. (A) Backbone RMSD of BCL-2, (B) RMSD profile of polyphenols.

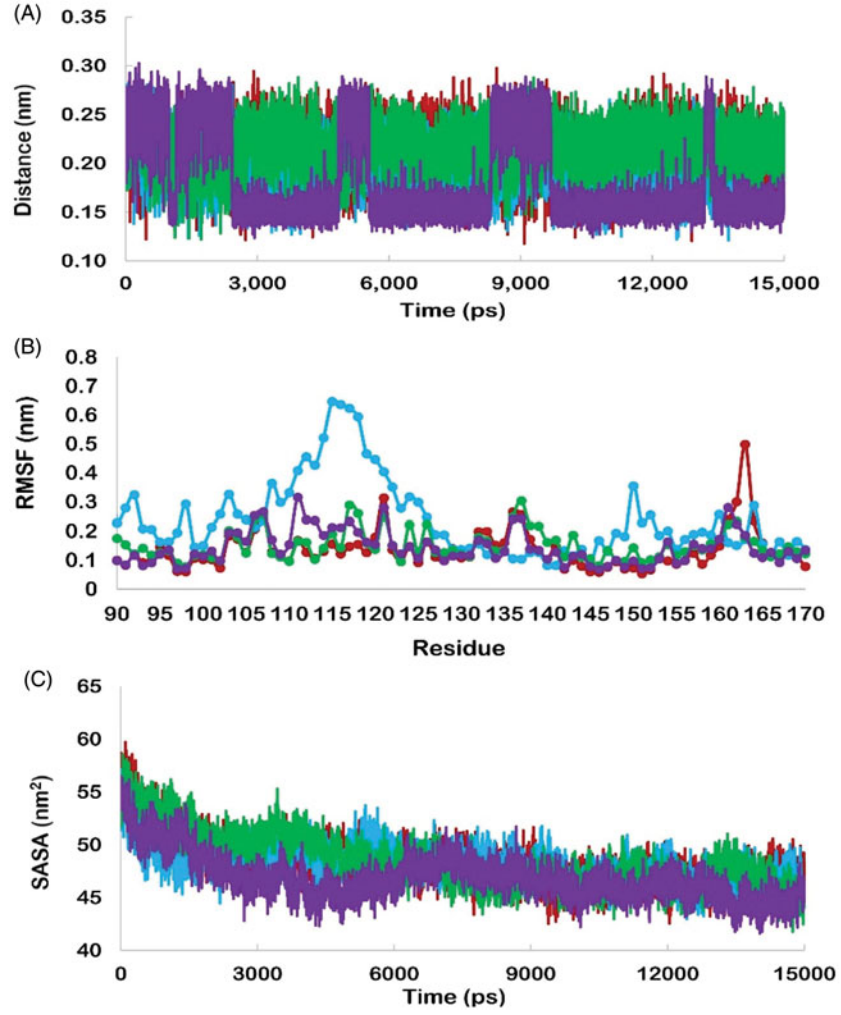

Figure 3. (A) Minimum distance profile between BCL-2 and polyphenols, (B) RMSF profile of BCL-2 residues, (C) SASA profile of BCL-2.

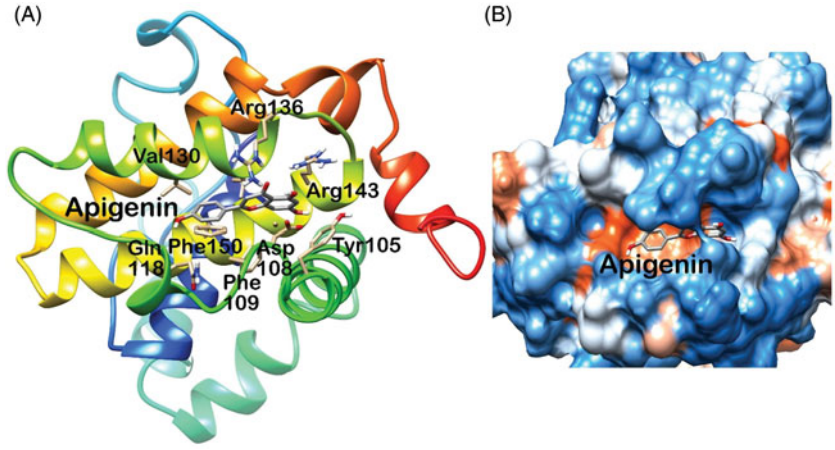

Figure 4. Apigenin-BCL-2 complex at 15 ns (A) cartoon representation, (B) surface structure.

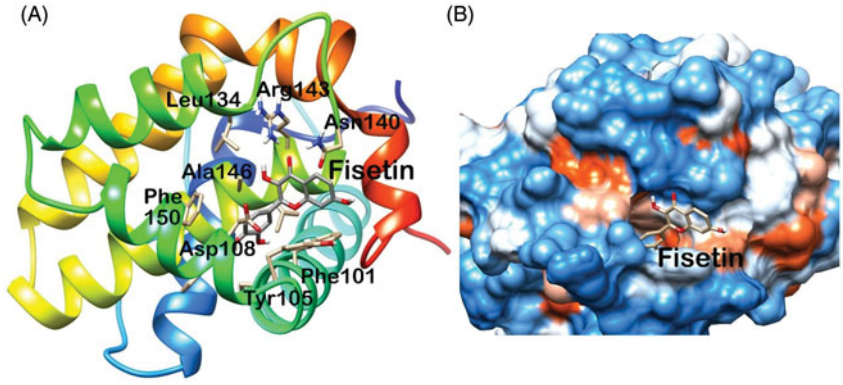

Figure 5. Fisetin–BCL-2 complex at 15 ns (A) cartoon representation, (B) surface structure.

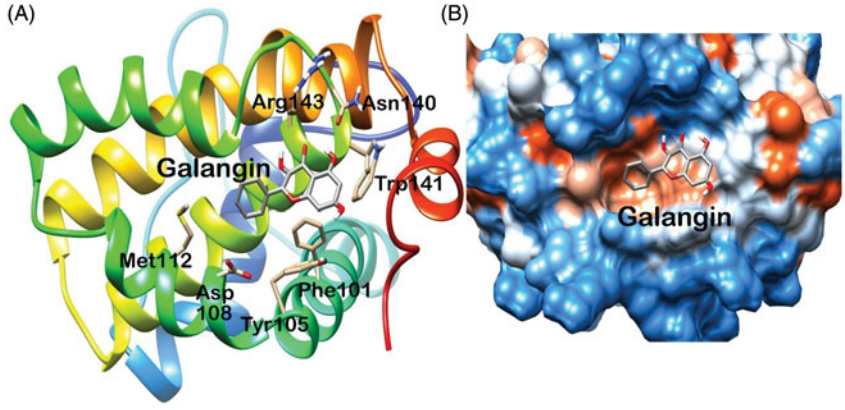

Figure 6. Galangin–BCL-2 complex at 15 ns (A) cartoon representation, (B) surface structure.

residues showed fluctuation within the range of 0.7 nm (Figure 3(B)). The Fisetin-bound BCL-2 showed higher fluctuation for residues 110–125 and 148–155 as compared to other polyphenol bound BCL-2. The bound fisetin was distant to these residues so they were free to move, while residues 134–140 were close to fisetin and showed less RMSF value as compared to other polyphenol bound BCL-2. Solvent accessible surface area (SASA) indicates the solvent-exposed surface of protein and hence, the folding of exposed part of proteins. All polyphenol-bound BCL-2 showed decreased SASA that may be associated with the conformational rearrangement (Figure 3(C)).

Analysis of final pose of BCL-2–ligand complex after 15 ns run of molecular dynamics simulation revealed that polyphenols stably bound to the hydrophobic groove. Figure 4 shows that apigenin is surrounded by the hydrophobic groove residues in the complex. Residues were found to cover the bound apigenin (Figure 4(B)). However, the binding site for all the polyphenols is more or less similar as shown in Figures 5, 6, and 7, respectively. Fisetin and luteolin

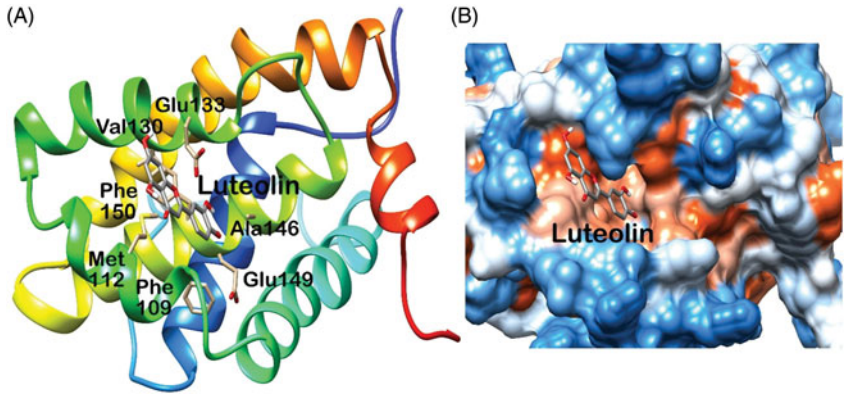

Figure 7. Luteolin–BCL-2 complex at 15 ns (A) cartoon representation, (B) surface structure.

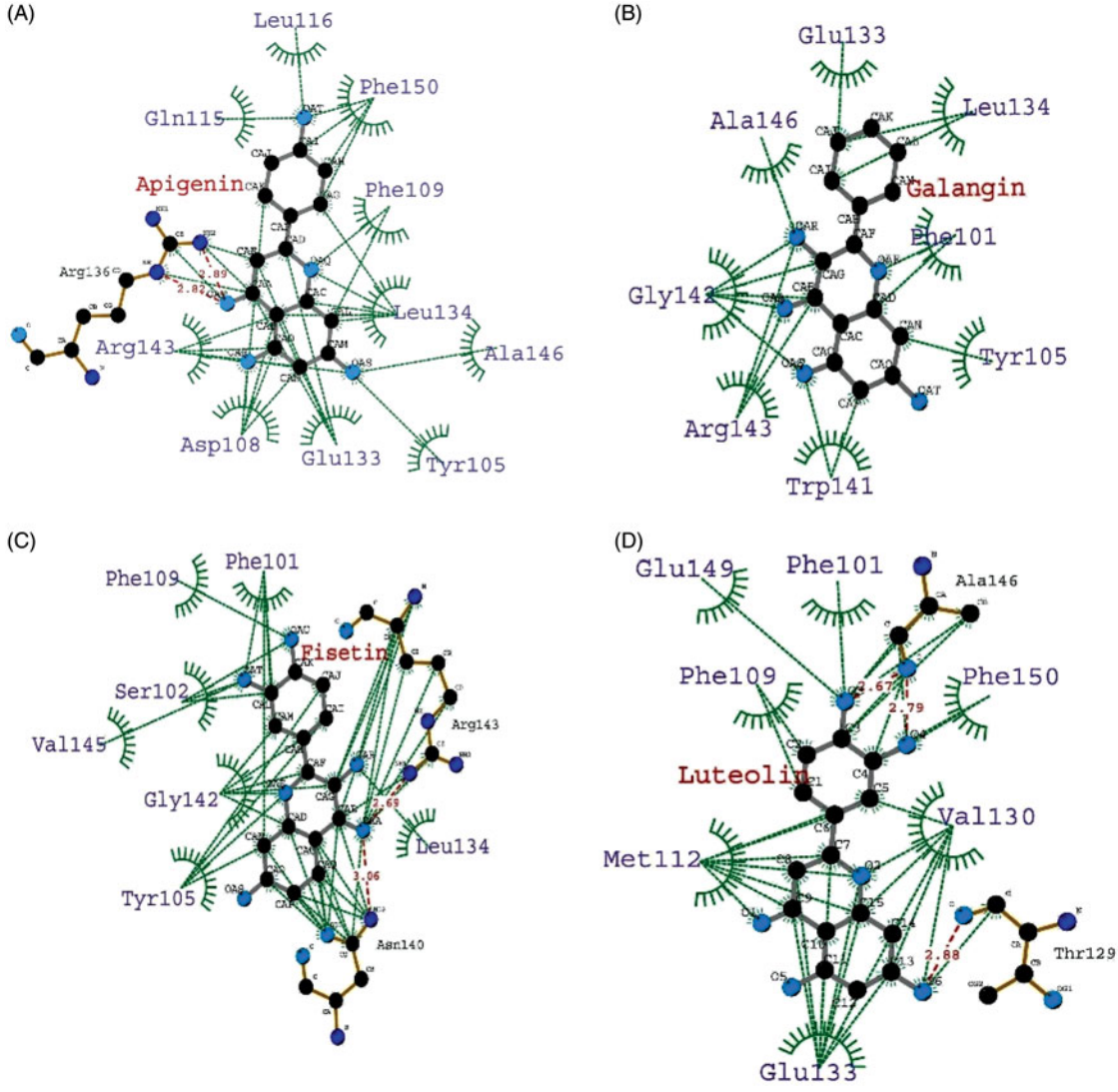

Figure 8. Polyphenol–BCL-2 interaction plot generated by Ligplot (A) Apigenin, (B) Galangin, (C) Fisetin, (D) Luteolin.

brought more significant change in the hydrophobic groove and were found to be deeply penetrated in the groove. These polyphenols induced deep pore-like structure and accommodated in it. Galangin was found stable at the binding site but did not penetrate in the groove. The interaction plot, generated by Ligplot (57), showed substantial hydrophobic interaction between residues and polyphenols. The interacting residues include Tyr105, Phe109, Glu133, Leu134 and Phe150 (Figure 8).

Free energy calculations

The binding free energy components obtained from the MM/PBSA calculation of the BCL-2-polyphenol complexes are

Table 1. MM/PBSA Free energy calculation of BCL2–polyphenol complexes.

Ligands	MM energy (vdW + Electrostatic) (kJ/mol)	Polar solvation (kJ/mol)	SASA (kJ/mol)	Binding energy (kJ/mol)
Apigenin	−170.29	66.49	−11.80	−115.6
Fisetin	−194.06	58.96	−14.31	−149.41
Galangin	−161.20	64.05	−12.73	−109.88
Luteolin	−223.20	60.05	−11.79	−174.94

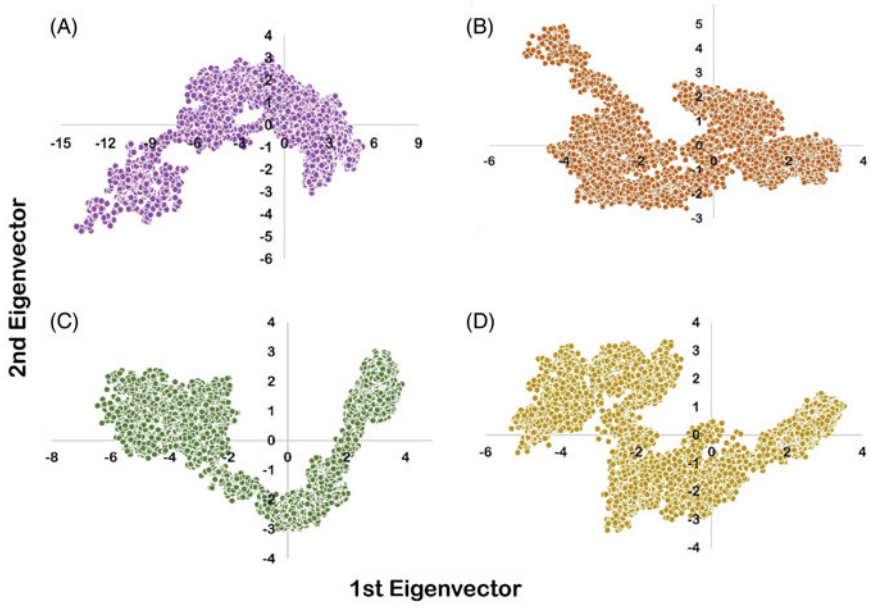

Figure 9. Polyphenol-bound BCL-2 in phase space along the first two eigenvectors (A) Apigenin, (B) Galangin, (C) Fisetin, (D) Luteolin.

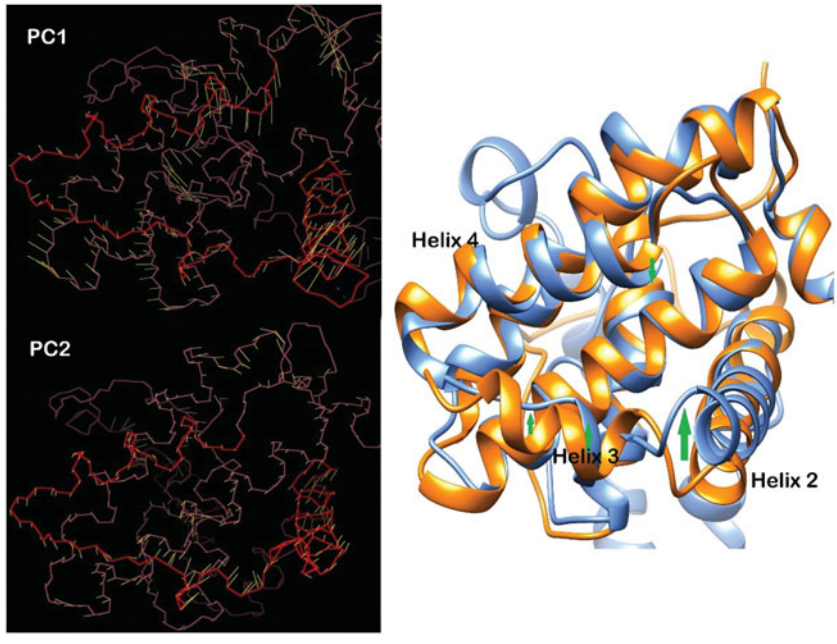

Figure 10. Apigenin bound BCL-2 motions driven by first two principal component (black background) and comparison of initial and average structure (after 15-ns simulation). Arrows are showing the motion of helices.

listed in Table 1. The results show that luteolin possessed the highest negative binding free energy with value of −174.94 kJ/mol followed by fisetin with a value of −149.41 kJ/mol. Apigenin and galangin showed affinity with values of −116.60 and −109.88 kJ/mol, respectively.

The van der Waals' interactions were found to give much larger contribution than electrostatic interactions for all BCL-2-polyphenol complexes. The nonpolar free energy contributes relatively less as compared to the total binding energy. The entropic term was not included in the calculations so

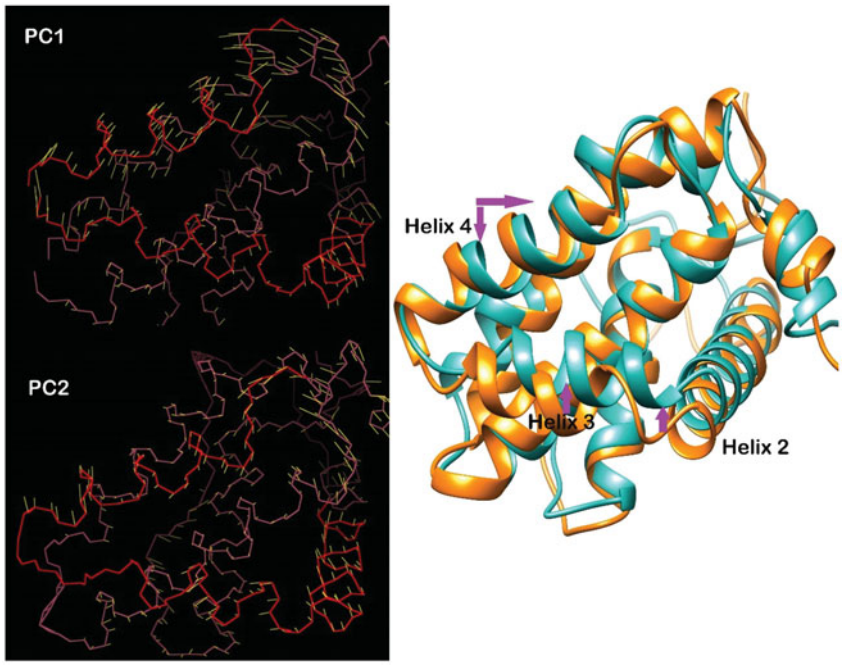

Figure 11. Fisetin-bound BCL-2 motions driven by first two principal component (black background) and comparison of initial and average structure (after 15-ns simulation). Arrows are showing the motion of helices.

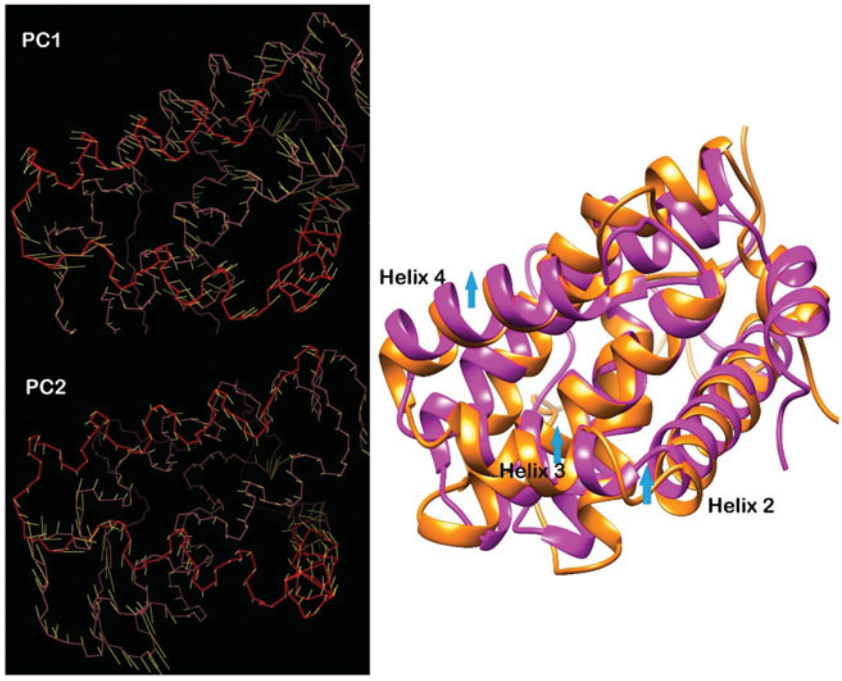

Figure 12. Galangin-bound BCL-2 motions driven by first two principal component (black background) and comparison of initial and average structure (after 15-ns simulation). Arrows are showing the motion of helices.

binding energy values will show some deviation. This indicates that nonpolar solvation energy, van der Waals and electrostatic interaction together contribute to the BCL-2–polyphenol complex stability. From the data collected by MM/PBSA calculations and the interaction plot generated by Ligplot, it is proved that hydrophobic interactions are dominant in all complexes. High negative value of vdW energy represents the massive hydrophobic interaction between BCL-2 and polyphenols.

Principal component analysis (PCA)

The MD trajectory of system was inspected with the principal components to better understand the conformational changes of the BCL-2 in all polyphenol bound forms. Collective motion of polyphenol bound BCL-2 was inspected by using phase space plots as shown in Figure 9. We projected MD trajectories on first principal component PC1 and PC2 for polyphenol bound BCL-2. As evident from Figure 9,

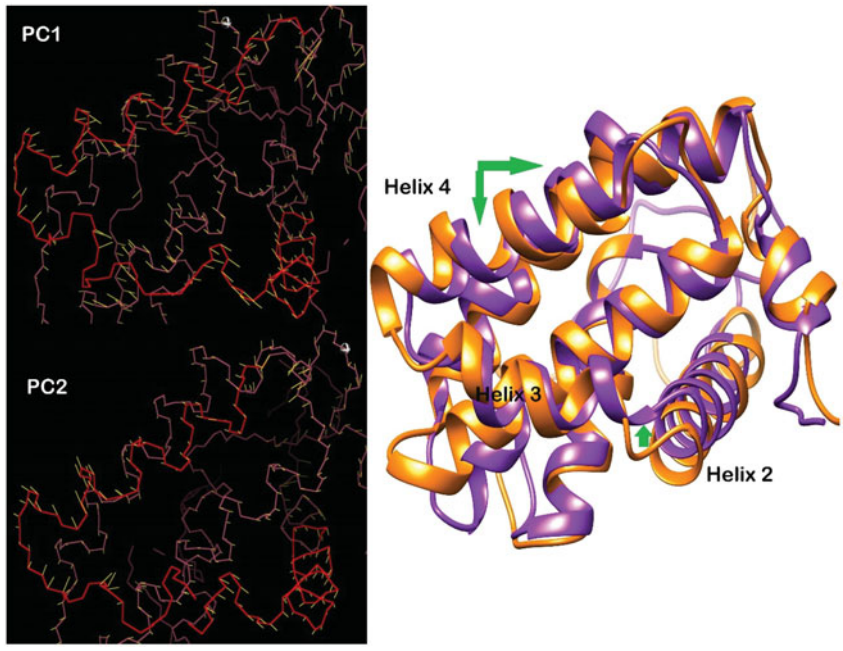

Figure 13. Luteolin-bound BCL-2 motions driven by first two principal component (black background) and comparison of initial and average structure (after 15-ns simulation). Arrows are showing the motion of helices.

dissimilar eigen values were observed in different polyphenol-bound BCL-2 due to conformational changes. This indicates conformational diversity of BCL-2. These motions collectively drive the structure of hydrophobic groove and also the intensity of hydrophobic interaction.

The first and second principal modes of dynamics of apigenin-bound BCL-2 are shown using spines in Figure 10. PC1 governed the motion of helix 4 and helix 2 downwards and upwards respectively. PC2 governed upward motion of helix 3. Comparison of initial structure with average structure of 15 ns simulation also revealed that motion of helices 2, 3 and 4 governed the structure of apigenin-bound BCL-2. PC1 and PC2 drive the protein to cover apigenin bound to the hydrophobic groove as revealed by final snapshot recorded at 15 ns. In case of fisetin-bound BCL-2, PC2 derived the motion of helices 2 and 3 toward the helix 4. Comparison of initial structure with average structure advocates in favor of PC2-derived motions (Figure 11). Galangin-bound BCL-2, however, showed different pattern of motions. Helices 2, 3 and 4 were in same direction which resulted in an uncovered bound galangin (as discussed earlier) (Figure 12). Luteolin bound form showed motions similar to fisetin, but helix 3 slightly moved downwards (Figure 13). All these motions drive the conformational changes induced by ligand binding.

Conclusions

All polyphenols (apigenin, fisetin, galangin and luteolin) bind to hydrophobic groove of BCL-2 and the binding was stable throughout MD simulation. Luteolin bound with highest negative binding energy and claimed highest potency towards BCL-2 inhibition. However, the BCL-2 interacting residues were found nearly similar for all polyphenols, but the change in groove structure significantly affected the position of polyphenol in groove and also the binding energy. The hydrophobic interactions were critical for stable complex formation as revealed by the vdW energy and ligplot analysis. Finally, on the basis of data obtained during the study, it can be concluded that these polyphenols have potential to be used as lead molecule for the inhibition of BCL-2.

Acknowledgements

AG is grateful to University Grants Commission, India for the Faculty Recharge Position. SV is thankful of Council of Scientific and Industrial Research (CSIR), India, for providing senior research associateship (pool scientist scheme).

Disclosure statement

The authors report no conflicts of interest. The authors alone are responsible for the content and writing of this article.

References

1. Igney FH, Krammer PH. Death and anti-death: tumour resistance to apoptosis. Nat Rev Cancer 2002;2:277–88.
2. Reed JC. Apoptosis-based therapies. Nat Rev Drug Discov 2002;1:111–21.
3. Pinto M, Perez JJ, Rubio-Martinez J. Molecular dynamics study of peptide segments of the BH3 domain of the proapoptotic proteins Bak, Bax, Bid and Hrk bound to the Bcl-xL and Bcl-2 proteins. J Comput-Aided Mol Des 2004;18:13–22.
4. Adams JM, Cory S. Life-or-death decisions by the Bcl-2 protein family. Trends Biochem Sci 2001;26:61–6.
5. Cao X, Yap JL, Newell-Rogers MK, et al. The novel BH3 alpha-helix mimetic JY-1-106 induces apoptosis in a subset of cancer cells (lung cancer, colon cancer and mesothelioma) by disrupting Bcl-xL and Mcl-1 protein-protein interactions with Bak. Mol Cancer 2013;12:42.

6. Czabotar PE, Lessene G, Strasser A, Adams JM. Control of apoptosis by the BCL-2 protein family: implications for physiology and therapy. Nat Rev Mol Cell Biol 2014;15:49–63.
7. Hosseini A, Espona-Fiedler M, Soto-Cerrato V, et al. Molecular interactions of prodiginines with the BH3 domain of anti-apoptotic Bcl-2 family members. PLoS One 2013;8:e57562.
8. Opferman JT, Korsmeyer SJ. Apoptosis in the development and maintenance of the immune system. Nat Immunol 2003;4:410–15.
9. Kim H, Rafiuddin-Shah M, Tu H-C, et al. Hierarchical regulation of mitochondrion-dependent apoptosis by BCL-2 subfamilies. Nat Cell Biol 2006;8:1348–58.
10. Willis SN, Fletcher JI, Kaufmann T, et al. Apoptosis initiated when BH3 ligands engage multiple Bcl-2 homologs, not Bax or Bak. Science 2007;315:856–9.
11. Antignani A, Youle RJ. How do Bax and Bak lead to permeabilization of the outer mitochondrial membrane? Curr Opin Cell Biol 2006;18:685–9.
12. Green DR, Kroemer G. The pathophysiology of mitochondrial cell death. Science 2004;305:626–9.
13. Ku B, Liang C, Jung JU, Oh B-H. Evidence that inhibition of BAX activation by BCL-2 involves its tight and preferential interaction with the BH3 domain of BAX. Cell Res 2011;21:627–41.
14. Liu X, Dai S, Zhu Y, et al. The structure of a Bcl-xL/Bim fragment complex: implications for Bim function. Immunity 2003;19:341–52.
15. Maity A, Yadav S, Verma CS, Dastidar SG. Dynamics of Bcl-xL in water and membrane: molecular simulations. PLoS One 2013;8:e76837.
16. Petros AM, Nettesheim DG, Wang Y, et al. Rationale for Bcl-XL/Bad peptide complex formation from structure, mutagenesis, and biophysical studies. Protein Sci 2000;9:2528–34.
17. Sattler M, Liang H, Nettesheim D, et al. Structure of Bcl-xL-Bak peptide complex: recognition between regulators of apoptosis. Science 1997;275:983–6.
18. Dlugosz PJ, Billen LP, Annis MG, et al. Bcl-2 changes conformation to inhibit Bax oligomerization. EMBO J 2006;25:2287–96.
19. Lin B, Kolluri SK, Lin F, et al. Conversion of Bcl-2 from protector to killer by interaction with nuclear orphan receptor Nur77/TR3. Cell 2004;116:527–40.
20. Wang K, Gross A, Waksman G, Korsmeyer SJ. Mutagenesis of the BH3 domain of BAX identifies residues critical for dimerization and killing. Mol Cell Biol 1998;18:6083–9.
21. Yin X-M, Oltvai ZN, Korsmeyer SJ. BH1 and BH2 domains of Bcl-2 are required for inhibition of apoptosis and heterodimerization with Bax. Nature 1994;369:321–3.
22. Zha H, Aimé-Sempé C, Sato T, Reed JC. Proapoptotic protein Bax heterodimerizes with Bcl-2 and homodimerizes with Bax via a novel domain (BH3) distinct from BH1 and BH2. J Biol Chem 1996;271:7440–4.
23. Ding J, Zhang Z, Roberts GJ, et al. Bcl-2 and Bax interact via the BH1–3 groove-BH3 motif interface and a novel interface involving the BH4 motif. J Biol Chem 2010;285:28749–63.
24. Suzuki M, Youle RJ, Tjandra N. Structure of Bax: coregulation of dimer formation and intracellular localization. Cell 2000;103:645–54.
25. Petros AM, Olejniczak ET, Fesik SW. Structural biology of the Bcl-2 family of proteins. Biochimica Et Biophysica Acta (BBA)-Mol Cell Res 2004;1644:83–94.
26. Day CL, Chen L, Richardson SJ, et al. Solution structure of prosurvival Mcl-1 and characterization of its binding by proapoptotic BH3-only ligands. J Biol Chem 2005;280:4738–44.
27. Acoca S, Cui Q, Shore GC, Purisima EO. Molecular dynamics study of small molecule inhibitors of the Bcl-2 family. Proteins Struct Funct Bioinf 2011;79:2624–36.
28. Birt D, Mitchell D, Gold B, et al. Inhibition of ultraviolet light induced skin carcinogenesis in SKH-1 mice by apigenin, a plant flavonoid. Anticancer Res 1996;17:85–91.
29. Kimira M, Arai Y, Shimoi K, Watanabe S. Japanese intake of flavonoids and isoflavonoids from foods. J Epidemiol 1998;8:168–75.
30. Miyajima Y, Kikuzaki H, Hisamoto M, Nakatani N. Antioxidative polyphenols from berries of Pimenta dioica. Biofactors 2004;22:301–3.
31. Seelinger G, Merfort I, Wölfle U, Schempp CM. Anti-carcinogenic effects of the flavonoid luteolin. Molecules 2008;13:2628–51.
32. Lin Y, Shi R, Wang X, Shen HM. Luteolin, a flavonoid with potential for cancer prevention and therapy. Curr Cancer Drug Targets 2008;8:634.
33. Verma S, Singh A, Mishra A. Complex disruption effect of natural polyphenols on Bcl-2-Bax: molecular dynamics simulation and essential dynamics study. J Biomol Struct Dynamics 2015;33:1094–106.
34. Dhanjal JK, Grover S, Sharma S, et al. Structural insights into mode of actions of novel natural Mycobacterium protein tyrosine phosphatase B inhibitors. BMC Genom 2014;15:S3.
35. Goyal M, Dhanjal JK, Goyal S, et al. Development of dual inhibitors against Alzheimer's disease using fragment-based QSAR and molecular docking. BioMed Res Int 2014;2014:979606.
36. Maindola P, Jamal S, Grover A. Cheminformatics based machine learning models for AMA1-RON2 abrogators for inhibiting plasmodium falciparum erythrocyte invasion. Mol Inform 2015;34:655–64.
37. Patel K, Tyagi C, Goyal S, et al. Curcumin-based IKKβ inhibiting anticancer lead design using novel fragment-based group QSAR modelling. Med Chem Res 24:2022–32.
38. Patel K, Tyagi C, Goyal S, et al. Identification of chebulinic acid as potent natural inhibitor of M. tuberculosis DNA gyrase and molecular insights into its binding mode of action. Comput Biol Chem 2015;59:37–47.
39. Sinha S, Tyagi C, Goyal S, et al. Fragment based G-QSAR and molecular dynamics based mechanistic simulations into hydroxamic-based HDAC inhibitors against spinocerebellar ataxia. J Biomol Struct Dyn 2015;34:1–39.
40. Tyagi C, Bathke J, Goyal S, et al. Targeting the intersubunit cavity of Plasmodium falciparum glutathione reductase by a novel natural inhibitor: Computational and experimental evidence. Int J Biochem Cell Biol 2015;61:72–80.
41. Tyagi C, Gupta A, Goyal S, et al. Fragment based group QSAR and molecular dynamics mechanistic studies on arylthioindole derivatives targeting the α-β interfacial site of human tubulin. BMC Genomics 2014;15:S3.
42. Vats C, Dhanjal JK, Goyal S, et al. Computational design of novel flavonoid analogues as potential AChE inhibitors: analysis using group-based QSAR, molecular docking and molecular dynamics simulations. Struct Chem 2015;26:467–76.
43. Oltersdorf T, Elmore SW, Shoemaker AR, et al. An inhibitor of Bcl-2 family proteins induces regression of solid tumours. Nature 2005;435:677–81.
44. Morris GM, Goodsell DS, Halliday RS, et al. Automated docking using a Lamarckian genetic algorithm and an empirical binding free energy function. J Comput Chem 1998;19:1639–62.
45. Morris GM, Huey R, Lindstrom W, et al. AutoDock4 and AutoDockTools4: Automated docking with selective receptor flexibility. J Comput Chem 2009;30:2785–91.
46. Berendsen HJ, van der Spoel D, van Drunen R. GROMACS: a message-passing parallel molecular dynamics implementation. Comput Phys Commun 1995;91:43–56.
47. Lindahl E, Hess B, Van Der Spoel D. GROMACS 3.0: a package for molecular simulation and trajectory analysis. J Mol Model 2001;7:306–17.
48. SchuÈttelkopf AW, Van Aalten DM. PRODRG: a tool for high-throughput crystallography of protein–ligand complexes. Acta Crystallogr Sect D Biol Crystallogr 2004;60:1355–63.
49. van Gunsteren WF, Billeter S, Eising A, et al. 1996. Biomolecular simulation: The {GROMOS96} manual and user guide.
50. van Gunsteren WF, Daura X, Mark AE. GROMOS force field. Encyclopedia of computational chemistry. 1998;2:1211–16.
51. Pettersen EF, Goddard TD, Huang CC, et al. UCSF Chimera—a visualization system for exploratory research and analysis. J Comput Chem 2004;25:1605–12.
52. Kollman PA, Massova I, Reyes C, et al. Calculating structures and free energies of complex molecules: combining molecular

mechanics and continuum models. Acc Chem Res 2000; 33:889–97.
53. Kumari R, Kumar R, Lynn A. g_mmpbsa-a GROMACS tool for high-throughput MM-PBSA calculations. J Chem Inform Model 2014;54:1951–62.
54. Homeyer N, Gohlke H. Free energy calculations by the molecular mechanics Poisson-Boltzmann surface area method. Mol Informat 2012;31:114–22.
55. Van Aalten D, Findlay J, Amadei A, Berendsen H. Essential dynamics of the cellular retinol-binding protein-evidence for ligand-induced conformational changes. Protein Eng 1995;8: 1129–35.
56. DeLano WL. 2002. The PyMOL molecular graphics system.
57. Wallace AC, Laskowski RA, Thornton JM. LIGPLOT: a program to generate schematic diagrams of protein-ligand interactions. Protein Eng 1995;8:127–34.